Advances in Aerospace Science and Applications.
Volume 8, Number 2 (2018), pp. 99-112

http://www.ripublication.com

Gabbard Diagram Formation: The General Theory for Elliptical Orbits

Robert C. Reynolds[1], Arjun Tan* and Marius Schamschula

Department of Physics, Alabama A & M University, Normal, AL 35762, U. S. A.
[1]VP for Advanced Programs, STAR Dynamics Inc., Hilliard, OH 43026, U.S.A.

Abstract

In a previous study, the theory of Gabbard diagram formation for fragments of a satellite breakup in circular orbit was presented including the 'X' formation, the equations of the apogee and perigee lines, the forbidden zone, the smear of points above and below the X, and the equation of the hyperbolic envelopes of the points obtained. The magnitudes of the limiting velocity perturbations in the down-range and radial directions were estimated from that diagram. The current study extends the theory of formation of the Gabbard diagram to satellite fragmentations in elliptical orbits. The slopes of the apogee and perigee lines are obtained and the condition of parallelism of the lines determined. The dependences of the Gabbard diagram on the eccentricity of the orbit and true anomaly of the fragmenting satellite are discussed. The results reduce to those for circular orbits for the limiting case of vanishing eccentricity.

1. INTRODUCTION

The ***Gabbard diagram*** is a simple yet useful tool now-a-days employed in virtually all satellite fragmentation studies. It was invented by John Gabbard, then at North American Aerospace Defense Command (NORAD/ADCOM) in the early years of satellite fragmentation history [1]. It plots the apogee and perigee heights of the fragmenting satellite and its fragments against their orbital periods. Constructing the Gabbard diagram of any satellite fragmentation event is invariably the first order of business to learn or confirm about the specifics of the event, e.g., the nature of the orbit, the location of the fragmentation point, the directionality and intensity of the fragments' spread, etc. In The Satellite Fragmentation Catalog [2], Gabbard diagrams of each and all fragmentation event are shown. Gabbard diagrams of circular, nearly circular, elliptic or highly elliptic orbits have characteristic features depending upon the location of the fragmentation in orbit. Illustrative examples of the various types of Gabbard diagrams are found in references [3 − 5].

For fragmentation from a circular orbit, the Gabbard diagram has the shape of an '***inclined X***' formed by a horizontal straight line and a straight line having a positive slope, the two lines intersecting at the coordinates of the fragmenting satellite (P_0, h_0). The right hand side of the X, to the right of (P_0, h_0), is generally created by posigrade impulses to the fragments (down-range velocity change $dv_d > 0$) while the left hand side of the X is normally generated by retrograde impulses to the fragments ($dv_d < 0$). Ideally, for an isotropic fragmentation of a satellite in a circular orbit, the Gabbard diagram will have a symmetric spread about (P_0, h_0). In the absence of radial velocity changes (dv_r), the apogee and perigee points lie on the two straight lines. The effect of dv_r is to shift points above and below the apogee and perigee lines, creating a '***halo***'-like appearance contained between two ***hyperbolic envelopes*** above and below the apsidal lines. The angular space between the two lines is, ideally devoid of fragments and represents a '***forbidden zone***'. The Gabbard diagram does not depend upon the cross-range velocity changes (dv_x).

2. Gabbard Diagram Formation for Satellite Fragmentation in Circular Orbits

For the problem at hand, it is found suitable to review the formation of the Gabbard diagram for fragmentation in circular orbits first and generalize it to elliptical orbits thereupon. In the Gabbard diagram, the independent variable is the orbital period P of the fragmenting satellite and its fragments. By Kepler's harmonic law, P is directly related to the semi-major axis a, of the satellite:

$$P^2 = \frac{4\pi^2}{\mu} a^3 \tag{1}$$

where μ is the gravitational parameter of the Earth. Taking differentials, one gets

$$dP = \frac{3P}{2a} da \tag{2}$$

Thus, a change in the semi-major axis of a fragment is directly proportional to the change in its orbital period. P is also related to the specific total energy of the orbit E by the relation:

$$P^2 = \frac{\pi^2 \mu^2}{2E^3} \tag{3}$$

Taking differentials, likewise, we get

$$dP = -\frac{3P}{2E} dE = \frac{3P}{2E}(-dE) \tag{4}$$

Since E is negative for bound Keplerian orbits, $-dE$ is a positive quantity. Thus P is also directly related to E. Equations (2) and (4), therefore reveal that P, a, and E, are all directly related to one another.

Dynamical variables in space must be defined in an inertial system of coordinates. A spacecraft local inertial system can be obtained from an Earth-centered inertial system by translation and rotations. An appropriate system to study the three ***orthogonal components*** of the ***velocity perturbation*** of a fragment is the following: (1) the ***radial component*** dv_r in the direction of the local vertical; (2) the ***down-range component*** dv_d along the local horizontal line in the plane of the orbit; and (3) the ***cross-range component*** dv_x in the direction of the orbital angular momentum of the fragmenting satellite. In that system, the velocity of the parent satellite is (v_r, v_d, 0); and that of the fragment is ($v_r + dv_r$, $v_d + dv_d$, dv_x). Whereas dv_r and dv_d produce changes in the orbital elements of the fragment in the parent's orbital plane, and therefore affect the Gabbard diagram, dv_x alters the plane of the fragment but does not affect the Gabbard diagram. The role of the latter is henceforth disregarded in this study.

The specific total energy of the fragment prior to the fragmentation (when it was still a part of the fragmenting satellite) is:

$$E = \frac{1}{2}\left[v_r^2 + v_d^2\right] - \frac{\mu}{r} \tag{5}$$

where μ is the gravitational parameter of the Earth and r is the radial distance of the fragmentation point from the center of the Earth. The specific total energy of the fragment upon fragmentation is:

$$E + dE = \frac{1}{2}\left[\left(v_r + dv_r\right)^2 + \left(v_d + dv_d\right)^2 + dv_x^2\right] - \frac{\mu}{r} \tag{6}$$

The change in specific energy of the fragment is, from Eqs. (5) and (6):

$$dE = v_d dv_d + v_r dv_r + \frac{1}{2}\left(dv_r^2 + dv_d^2 + dv_x^2\right) \tag{7}$$

Since the first term on the right of Eq. (7) is overwhelmingly greater than the rest, particularly for a near-circular orbit, we can write for orbits of small eccentricities:

$$dE \approx v_d dv_d \tag{8}$$

Thus, for all practical purposes, dv_d dictates dE and therefore dP by virtue of Eq. (4).

In general, dv_r and dv_d both produce changes in the semi-major axis da and eccentricity de in accordance with ***Lagrange's planetary equations*** [6]:

$$da = \frac{2}{n}\left[\frac{e\sin\theta}{\sqrt{1-e^2}}dv_r + \frac{a\sqrt{1-e^2}}{r}dv_d\right] \tag{9}$$

and

$$de = \frac{\sqrt{1-e^2}}{na}\left[\sin\theta dv_r + \left(1 - e^2 - \frac{r^2}{a^2}\right)dv_d\right] \tag{10}$$

In the above equations, a is the semi major axis of the parent satellite, e its eccentricity, n its mean motion, and θ its true anomaly at the fragmentation point.

The changes to the apogee height h_a and perigee height h_p are given by [7]:

$$dh_a = (1+e)da + ade \tag{11}$$

and

$$dh_p = (1-e)da - ade \tag{12}$$

respectively. Substituting from Eqs. (9) and (10), and setting e = 0, we obtain for circular orbits:

$$dh_a = \frac{2}{n} dv_d + \frac{\sin\theta}{n} dv_r \tag{13}$$

and

$$dh_p = \frac{2}{n} dv_d - \frac{\sin\theta}{n} dv_r \tag{14}$$

If $dv_d > 0$, the fragment attains a higher energy orbit, and the change in period $dP > 0$. However, the ***Hohmann transfer principle*** dictates that h_p is unaffected by dv_d.. Thus Eqs. (13) and (14) are re-written as

$$dh_a = \frac{2}{n} dv_d + \frac{\sin\theta}{n} dv_r \tag{15}$$

and

$$dh_p = -\frac{\sin\theta}{n} dv_r \tag{16}$$

Since dv_d alone alters a [vide Eq. (8)] and hence P, in the absence of dv_r, the perigee points lie on a horizontal straight line and the apogee points lie vertically above the perigee points on a straight line with positive slope. The effect of dv_r is then to move the apogee and perigee points above and below the apogee and perigee lines, respectively by the same distance given by the last terms of Eqs. (15) and (16), respectively. This describes the construction of the right hand side of the Gabbard diagram.

If, on the other hand, $dv_d < 0$, the fragment loses energy, and the change in period $dP <$ 0. In this case, the Hohmann transfer principle assures that h_a remains the same. Then Eqs. (13) and (14) are re-written as

$$dh_a = \frac{\sin\theta}{n} dv_r \tag{17}$$

and

$$dh_p = \frac{2}{n} dv_d - \frac{\sin\theta}{n} dv_r \tag{18}$$

In this case, the apogee points lie on a horizontal straight line and the perigee points lie vertically below the apogee lines on the inclined straight line. The effect of dv_r is again to move the apogee and perigee points above and below the apogee and perigee lines, respectively by the same distance given by the last terms of Eqs. (17) and (18). This explains the construction of the left hand side of the Gabbard diagram.

It is easy to see that the perigee line of the right hand side is identical to the apogee line of the left hand side, since both are horizontal lines passing through the same point (P_0, h_0). It has also been shown that the apogee line on the right hand side and the perigee line on the left hand side of the Gabbard diagram have the same slope [7]:

$$\left|\frac{dh_a}{dP}\right|_r = \left|\frac{dh_p}{dP}\right|_l = \frac{2da}{dP} = \frac{4a}{3P} \tag{19}$$

And, since both lines pass through (P_0, h_0), the two lines are coincident.

3. Gabbard Diagram Formation for Satellite Fragmentation in Elliptical Orbit

Gabbard diagrams for satellite fragmentations in elliptical orbits have more variety but are less spectacular than those in circular orbits. However, the basic principles of formation remain the same. In all cases, there are two apsidal lines which mark the boundaries of the '***forbidden zones***': (1) a ***horizontal line*** on which one apsis is located; and (2) a ***slant line*** on which the other apsis is situated. The slant line has a small upward curvature in consequence of Eq. (2). The two lines generally intersect when extended. The ***intersection point*** marks the period of a circular orbit for breakup at that altitude. Whether a fragment gains or loses period depends upon whether the total velocity of the fragment increases or decreases relative to that of the parent. But since this depends largely on the down-range velocity perturbation dv_d on account of Eq. (8), fragments to the right of the intersection point normally gain in energy, whereas those to the left of the intersection point normally lose energy. For fragments to the left of the intersection point (lower energy fragments), the lower line marks the maximum perigee for a fragment with that period; and for fragments to the right of the intersection point (higher period fragments), the upper line marks the maximum apogee for a fragment with that period.

Gabbard diagrams for satellite fragmentations in elliptical orbits depend on two primary factors: (1) ***eccentricity*** of the fragmenting satellite's orbit; and (2) ***true anomaly*** of the satellite at the point of fragmentation. Three case scenarios are discussed in this study: (1) when fragmentation occurs at apogee or perigee; (2) when fragmentation occurs between the apsidal points; and (3) when fragmentation takes place in a highly eccentric orbit ($e \geq .5$).

3.1. Fragmentation occurs near an Apsidal Point

When a satellite in an elliptical orbit fragments near its perigee, Hohmann transfer principle dictates that the perigee heights of the fragments remain the same while the apogee heights increase or decrease according to whether the downrange velocity perturbation is posigrade or retrograde. The Gabbard diagram is similar to the right hand side of that of a fragmentation in a circular orbit. For an isotropic fragmentation, there are approximately equal number of points to the left and right of the parent satellite's location.

If the satellite fragments near its apogee, on the other hand, the apogee points of the fragments remain the same by the Hohmann transfer principle; and the perigee heights increase or decrease in accordance with posigrade or retrograde velocity perturbation in the down-range direction. The Gabbard diagram in this case resembles the left hand side of that of the 'X' pattern for circular orbits.

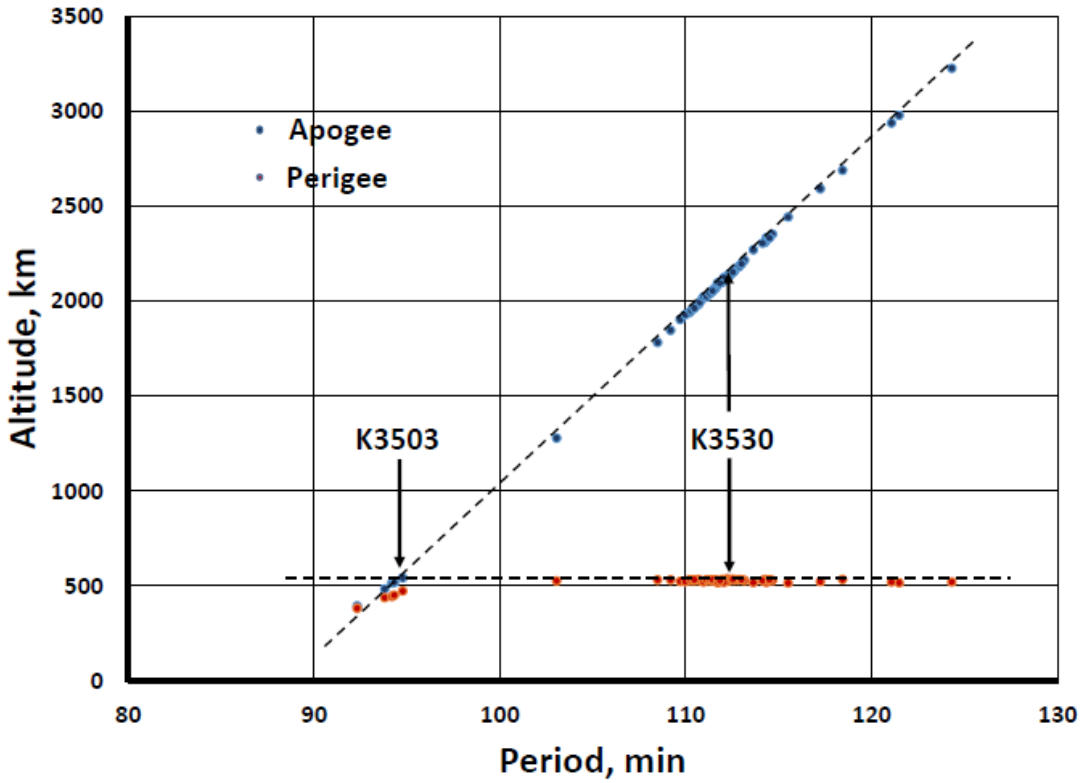

Fig. 1. Gabbard diagrams of K248 and K252 fragments.

Figure 1 shows the Gabbard diagrams of both of the above cases of fragmentations. It pertains to the first Soviet ASAT test against a live target in orbit. In October 1968, Cosmos 248 (K248) was launched into a near-circular orbit (eccentricity e = .005) to serve as the target satellite. A few days later, Cosmos 252 (K252) was launched into an elliptical orbit (eccentricity e = .104). At the rendezvous location (which was planned

to coincide with the apogee of K248 and the perigee of K252), the interceptor satellite K252 was deliberately exploded into over 100 trackable fragments, one of which then fragmented the target into four trackable pieces in consequence [8 – 11]. The combined Gabbard diagrams of the K248 and K252 fragments (Fig. 1) exhibit an 'X' form about the rendezvous altitude of 535 km and period of 94 min. The K252 fragments lie on the right hind side of the 'X' while the K248 fragment are located on the left hand side, with the latter showing obvious signs of atmospheric decay. The K252 fragment points lie almost evenly on either side of the fragmenting parent. The K248 orbit was nearly circular, even though the target was near its apogee.

3.2. The General Theory of Gabbard Diagram Formation

When the restriction of circular orbit ($e = 0$) is lifted, one can proceed with the general theory of Gabbard diagram formation. We continue with the notion that the structure of the apsidal lines are determined by dv_d's alone and the smear of points from the lines are the result of dv_r's. The apogee and perigee lines are determined by the down-range components in Eqs. (11) and (12):

$$\left|dh_a\right|_d = \left|(1+e)da + ade\right|_d \tag{20}$$

and

$$\left|dh_p\right|_d = \left|(1-e)da - ade\right|_d \tag{21}$$

where da and de are given by Eqs. (9) and (10). The results can be expressed in terms of the true anomaly θ of the fragmenting satellite by substitution by the equation of the orbit:

$$r = \frac{a\sqrt{1-e^2}}{1+e\cos\theta} \tag{22}$$

After considerable algebra, one arrives at:

$$\left|dh_a\right|_d = \frac{1+e}{n}\left[2(1+e\cos\theta) + \frac{(1-e)\cos\theta(2+e\cos\theta)}{1+e\cos\theta}\right]dv_d \tag{23}$$

and

$$\left|dh_p\right|_d = \frac{1-e}{n}\left[2(1+e\cos\theta) - \frac{(1+e)\cos\theta(2+e\cos\theta)}{1+e\cos\theta}\right]dv_d \tag{24}$$

Equation (23) and (24) define the apogee and perigee lines of the fragments, respectively.

The effects of the radial components of the velocity perturbations of the fragments are found from the following:

$$\left|dh_a\right|_r = \left|(1+e)da + ade\right|_r \tag{25}$$

and

$$\left|dh_p\right|_r = \left|(1-e)da - ade\right|_r \tag{26}$$

Upon similarly simplifying, we obtain:

$$\left|dh_a\right|_r = \frac{1}{n}\frac{(1+e)^2}{\sqrt{1-e^2}}\sin\theta dv_r \tag{27}$$

and

$$\left|dh_p\right|_r = -\frac{1}{n}\frac{(1-e)^2}{\sqrt{1-e^2}}\sin\theta dv_r \tag{28}$$

Equations (27) and (28) show that the apogee and perigee points are shifted above and below the apogee and perigee lines, respectively for ascending mode of the satellite ($0 < \theta < \pi$). Thus, the region between the apogee and perigee lines constitutes the '***forbidden zone***' for upward motion of the fragmenting satellite only. For downward motion of the satellite, the areas of the forbidden zones will lie above the apogee line and below the perigee line. Figure 2 is an example of the latter case. It is the Gabbard diagram of Himawari Delta second stage rocket which fragmented on 14 July 1977 while descending.

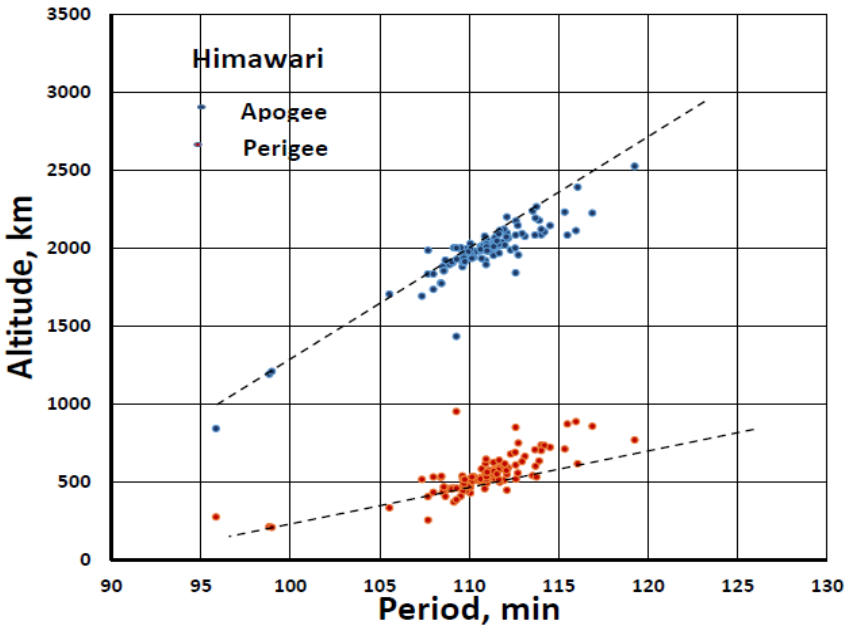

Fig. 2. Gabbard diagram of Himawari Rocket fragments.

Equations (23), (24), (27) and (28) comprise the general theory of Gabbard diagram formation for fragmentation in an elliptical orbit. They reduce to Eqs. (15) – (18) as a special case when $e \approx 0$.

3.3. Slopes of the Apogee and Perigee Lines

From the general properties of a Keplerian ellipse, we have [vide Eqs. (11) and (12)]:

$$dh_a + dh_p = 2da \tag{29}$$

Thus

$$\frac{dh_a}{dP} + \frac{dh_p}{dP} = \frac{2da}{dP} = \frac{4a}{3P} = m \tag{30}$$

where m is a constant. If α_a and α_p are the slope angles of the apogee and perigee lines, respectively, then

$$\tan\alpha_a + \tan\alpha_p = m \tag{31}$$

Equation (31) constitutes a '***theorem of conservation of slopes of the apsidal lines***'. The results of §3.1 show that: (1) When $\theta = 0$, $\alpha_a = m$, $\alpha_p = 0$; and (2) When $\theta = \pi$, $\alpha_a = 0$, $\alpha_p = m$. Thus, as the true anomaly θ is varied between 0 and π, α_a decreases as α_p increases. At some point, the two slope angles become equal, and the apogee and perigee lines become parallel. The condition of parallelism is given by $\alpha_a = \alpha_p$. Equating Eqs. (23) and (24), and simplifying, one gets a quadratic equation in $\cos\theta$:

$$e\left(e^2+1\right)\cos^2\theta + 2\left(e^2+1\right)\cos\theta + 2e = 0 \tag{32}$$

giving:

$$\cos\theta = \frac{-\left(e^2+1\right) \pm \sqrt{1-e^4}}{e\left(e^2+1\right)} \tag{33}$$

Retaining the upper sign only (the lower sign gives an unphysical solution), we obtain the true anomaly θ_0 for which the apogee and perigee lines have the same slope:

$$\theta_0 = \cos^{-1}\frac{-\left(e^2+1\right)+\sqrt{1-e^4}}{e\left(e^2+1\right)} \quad \text{or} \quad \theta_0 = 2\pi - \cos^{-1}\frac{-\left(e^2+1\right)+\sqrt{1-e^4}}{e\left(e^2+1\right)} \tag{34}$$

In Eq. (34), the first solution corresponds to the ascending mode of the fragmenting satellite and the second solution corresponds to the descending mode. The results for various eccentricities of the satellite orbit are shown in Table I. The dependence on the eccentricity is highly evident.

Table I. True anomaly θ at which slopes of apogee and perigee lines equal as functions of eccentricity e

Eccentricity e	θ_0 (ascending)	θ_0 (descending)
.1	95.71°	264.29°
.2	101.31°	258.69°
.3	106.72°	253.28°
.4	111.88°	248.12°
.5	116.80°	243.20°
.6	121.56°	238.44°
.7	126.63°	233.37°
.8	131.63°	228.37°
.9	138.69°	221.31°

Figure 3 depicts the various scenarios of Gabbard diagram formation. The dependence on the true anomaly of the fragmenting satellite is evident. The variation with eccentricity changes the value of θ_0, but not the general features. Figure 4 (from [12, 13]) betrays two of the five scenarios in Fig. 3. The left panel of Fig. 4 (from [13]) is the Gabbard diagram of K374 fragments which serves as an example for the upper right panel of Fig. 3. Likewise, the right panel of Fig. 4 (from [12]) is the Gabbard diagram of K249 fragments which corresponds to the lower left panel of Fig. 3. Both K249 and K374 were interceptor satellite which failed in their ASAT missions against the targets K248 and K373 respectively, and were exploded on command. The eccentricity of K249's orbit was .1088 and the true anomaly at breakup point was estimated as 146.38° [12]. Likewise, the eccentricity of K374's orbit was .1039 and the true anomaly was calculated to be 86.22° [13]. Both sets of information are consistent with Table I and Fig.3.

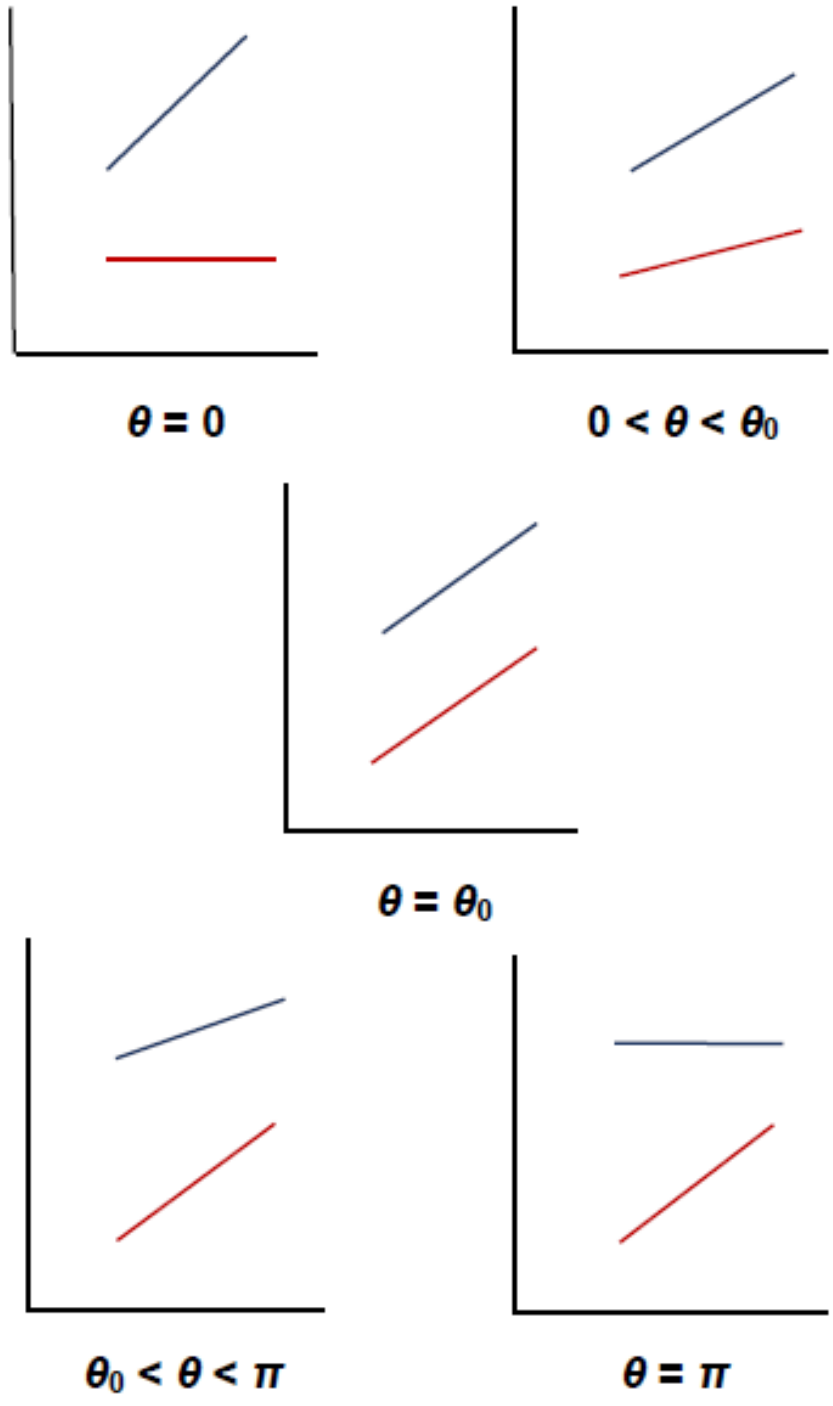

Fig. 3. Gabbard Diagrams for various true anomalies of the fragmenting satellite.

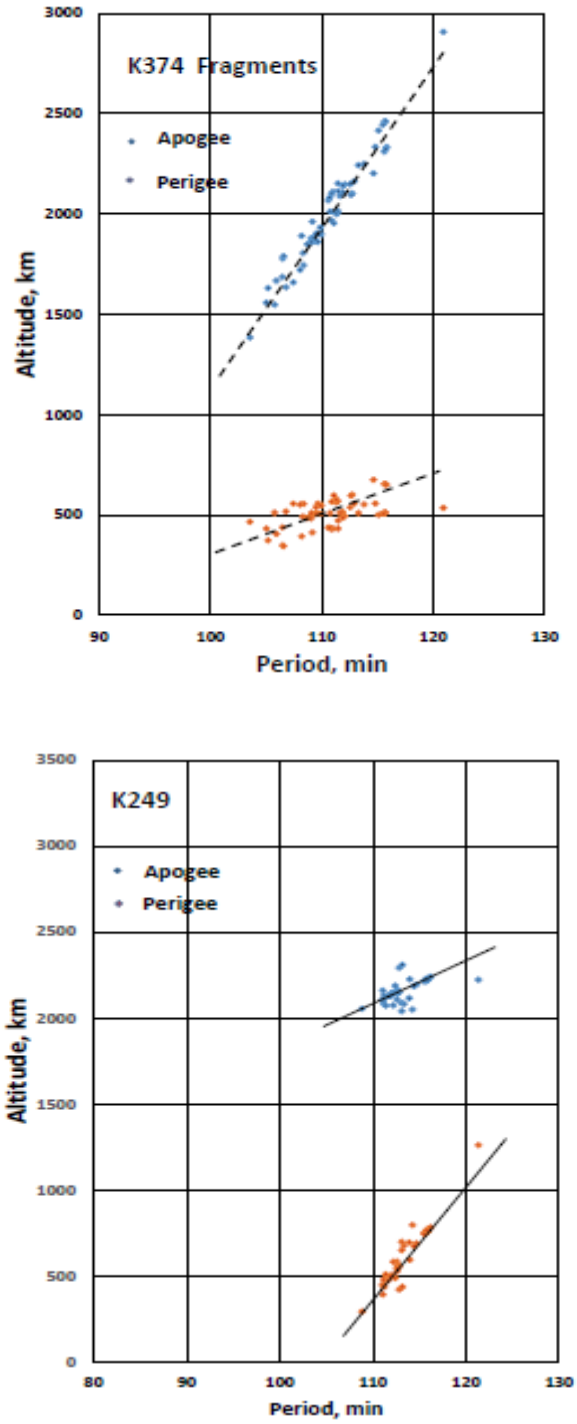

Fig. 4. Gabbard diagram of fragments of K374 and K259 killer satellites.

3.4. Fragmentation in highly Elliptical Orbit

When a satellite breaks up in a highly elliptical (eccentricities of .5 and above), the Gabbard diagram of the fragments is usually unspectacular and uninteresting. The slope of the perigee line is usually far smaller than that of the apogee line, and there is a large gap between the two. As a result, the perigee line lies at the bottom of the diagram with the apogee line situated high above it. Figure 5 (from [14]) is an example of such a Gabbard diagram which belonged to the fragments of a Briz-M rocket body (U.S. Satellite Number 28944) which suffered a massive explosion in 19 February 2007. It was in a highly eccentric orbit having eccentricity of .5083. Figure 5 includes the first 106 fragments cataloged through 1 January 2011.

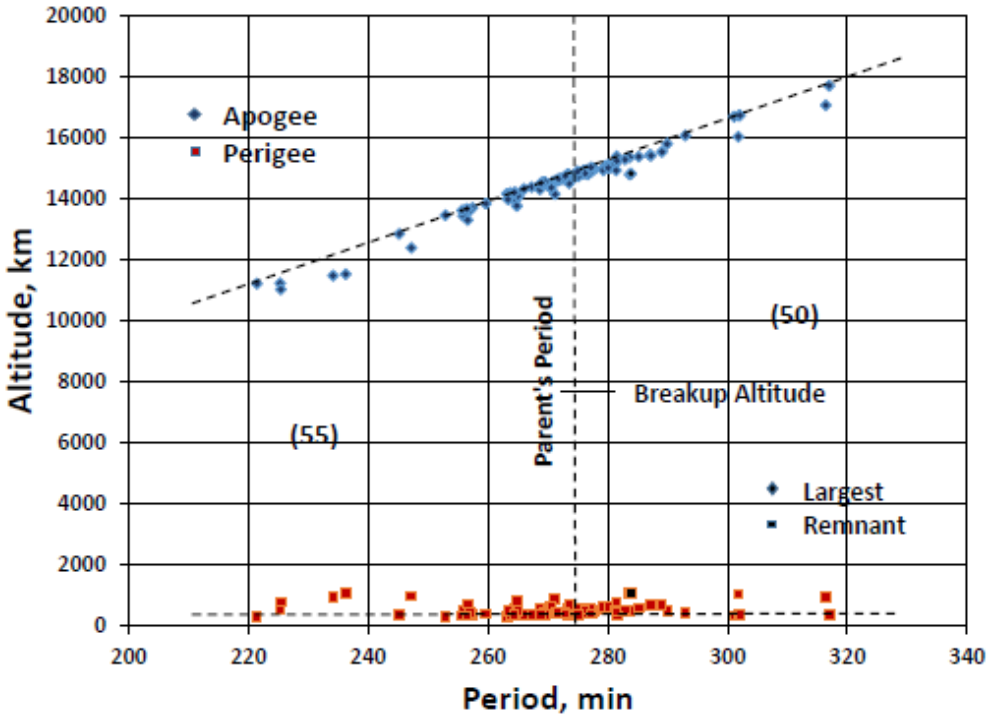

Fig. 5. Gabbard diagram of first 106 cataloged fragments of Briz-M rocket (28944).

4. CONCLUDING REMARKS

Since the dawn of satellite fragmentation studies, the Gabbard diagram has been an indispensable tool of analyzing satellite fragmentations in orbit. Yet, no theory of its formation had ever been undertaken until the authors published their ***special theory of Gabbard diagram formation*** for satellite fragmentations in circular orbits [7]. The current paper presents the ***general theory of Gabbard diagram formation*** for satellite fragmentations in elliptical orbits. This paper, in effect, concludes the theory of Gabbard diagram formation for satellite fragmentations in orbit.

REFERENCES

[1] J.R. Gabbard, *Explosion of Satellite 10704 and other Delta Second Stage Rockets*, **NORAD/ADCOM Tech. Memo, 81-5** (1981).

[2] N.L. Johnson, E. Stansbery, D.O. Whitlock, K.J. Abercromby & D. Shoots, *History of On-Orbit Satellite Fragmentations*, **NASA/TM-2008-214779** (2008).

[3] R.D. Culp, *Analysis of the Origins of Debris Clouds*, **Teledyne Brown Engg. Rept. Contract SC 7460** (1986).

[4] N.L. Johnson & D.S. McKnight, *Artificial Space Debris*, Krieger Publ. Co., Malabar, Florida (1991).

[5] M. Matney, https://ntrs.nasa.gov/archive/nasa/casi.ntrs.nasa.gov/20150009502.pdf.

[6] L. Meirovitch, *Methods of Analytical Dynamics*, McGraw-Hill, New York (1970).

[7] A. Tan, R.C. Reynolds & M. Schamschula, *NOAA-16 Satellite Fragmentation in Orbit: Genesis of the Gabbard Diagram and Estimation of the Intensity of Breakup*, **Adv. Aerospace Sci. Appl.**, **7**, 37-47 (2017).

[8] N.L. Johnson, Artificial Satellite Breakup (Part 2): Soviet Anti-Satellite Program, *J. Brit. Interplanet. Soc*., 36, 357-362 (1983).

[9] P.B. Stares, *Militarization of Space*, *U.S. Policy, 1945-1984*, Cornell University Press, Ithaca (1985).

[10] P.B. Stares, *Space and National Security*, Brookings Institution, Washington, (1987).

[11] Siddiqi, A.A. The Soviet Co-orbital Anti-satellite System: A Synopsis, *J. Brit. Interplanet. Soc*., *50*, 225-240 (1997).

[12] A. Tan, V. Edwards, & M. Schamschula, *Fragments Analyses of the Soviet Anti-Satellite Tests – Round 1*, **Adv. Aerospace Sci. & Appl**., **4**, 21-33 (2014).

[13] A. Tan, V. Edwards, & M. Schamschula, *Fragments Analyses of the Soviet Anti-Satellite Tests – Round 2*, **Adv. Aerospace Sci. & Appl**., **4**, 35-43 (2014).

[14] A. Tan, S. Sheng & M. Dokhanian, *Velocity Perturbations Analysis of the Briz-M Rocket (Arabsat-4A)*, **Adv. Aerospace Sci. Appl***.,* **4***,* 1-9 (2014).